ACS Photonics

Letter

pubs.acs.org/journal/apchd5

Optical Circulation and Isolation Based on Indirect Photonic Transitions of Guided Resonance Modes

Yu Shi,[†] Seunghoon Han,[‡] and Shanhui Fan*[,†]

[†]Department of Electrical Engineering, Ginzton Laboratory, Stanford University, Stanford, California 94305, United States

[‡]Samsung Advanced Institute of Technology, Samsung Electronics, Suwon 443-803, Korea

ABSTRACT: While there has been enormous progress in meta-surface designs, most meta-surfaces are constrained by Lorentz reciprocity. Breaking reciprocity, however, enables additional functionalities and greatly expands the applications of meta-surfaces. Here, we introduce a realistic nonreciprocal meta-surface that can achieve optical circulation and isolation. This device consists of a photonic crystal slab that supports two bands of guided resonances, and upon a temporal modulation in each unit cell with a spatially varying phase, an indirect photonic transition can be induced between the guided resonances, which breaks Lorentz reciprocity without the use of magneto-optic materials. We provide direct first-principle numerical simulations, using the multifrequency finite-difference frequency-domain method, to demonstrate that this device can achieve optical circulation and isolation with no back reflection under realistic modulation frequency and modulation strength.

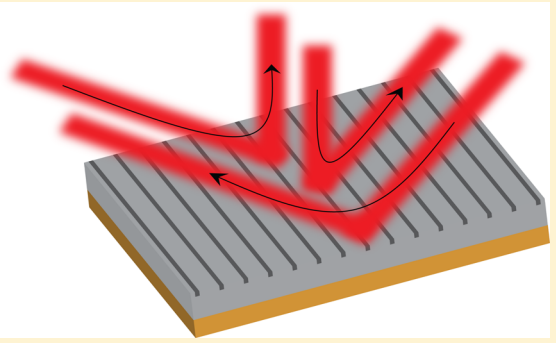

KEYWORDS: *metamaterials, optical isolation, dynamic modulation*

In recent years, there have been significant advancements in the manipulation of light using two-dimensional meta-materials, or meta-surfaces.[1−3] Meta-surfaces have been used in performing refraction and diffraction,[4−6] manipulating the polarization of light,[7,8] and realizing special optical physics on a two-dimensional platform, such as the generation of optical spin Hall effects[9] and optical vortices.[10] Moreover, there are now significant recent efforts in developing nonreciprocal meta-surfaces.[11−19] Breaking Lorentz reciprocity enables meta-surfaces to be used for important functionalities such as optical isolation and circulation, which are crucial in signal processing and for laser feedback protection and which cannot be realized in any reciprocal structures.[20−22]

There are two major approaches toward creating non-reciprocity that can be used to achieve complete optical isolation and circulation. Both approaches have been considered in meta-surfaces. The first method is to use magneto-optic materials.[11,12,23,24] Under a static magnetic field bias, magneto-optic materials exhibit a nonsymmetric permittivity tensor, which can be used in meta-surfaces to break the reciprocity between forward and backward propagating modes, resulting in optical isolation.[11,12] This approach can be purely passive, which is attractive. However, standard optoelectronic materials typically do not have magneto-optic effects, and consequently it is difficult to apply this approach in most standard optoelectronic platforms. The second method is to apply a dynamic modulation to the dielectric constant of the device. Such modulation also breaks reciprocity and can lead to complete optical isolation.[13,14,16,19,25−34] The dynamic modulation approach is an active approach that requires external energy input, but it is compatible with most standard optoelectronic materials. Therefore, there have been several recent proposals that use the dynamic modulation approach for constructing nonreciprocal meta-surfaces.[13,14,16,18,19]

In this paper, we focus on the dynamic modulation approach toward the creation of nonreciprocal meta-surfaces. In spite of the significant advancements as summarized above, there still remain significant challenges in realizing such dynamic nonreciprocal meta-surfaces in the optical frequency range. For example, one approach for achieving nonreciprocal response in dynamically modulated structures is based on the concept of photonic transition.[26−28,31−35] In this approach, one considers a photonic system supporting two optical modes at frequencies ω_1 and ω_2. Modulation of the system at a frequency $\Omega = \omega_1 - \omega_2$ can induce a photonic transition between these two optical modes. In such a transition, the upward and downward transition in frequency acquires opposite phases, which can be used to create nonreciprocal responses. There have been several attempts seeking to implement this concept in meta-surfaces.[13,14,16,18,19] However, there is a very large frequency difference between the modulation frequency and the optical frequency. The maximum modulation frequency typically used in electro-optic modulation is usually on the order of 10 GHz,[36] whereas a typically optical frequency is around 200 THz. A realistic design of a dynamic nonreciprocal meta-surface must take into account such a large frequency difference.

Received: April 24, 2017
Published: June 28, 2017

DOI: 10.1021/acsphotonics.7b00420
ACS Photonics 2017, 4, 1639−1645

In the present work, we introduce a design of a nonreciprocal meta-surface that operates in optical frequency while being driven by a refractive index modulation at tens of gigahertz based on the concept of photonic transition. This design incorporates two essential considerations. First, the device needs to have independent modes that are separated by an attainable modulation frequency of a few gigahertz. Second, these modes must have high enough quality factors so that they can be spectrally resolved. To meet these considerations, we exploit guided resonances in a photonic crystal slab. First, with a proper choice of the thickness of the slab, the slab supports guided resonances forming multiple photonic bands, and as a result, for a given modulation frequency Ω, it is always possible to find two optical modes in the structure with their frequencies differing by Ω. Second, with a proper choice of slab parameters, these guided resonances can achieve high quality factors. Thus, the photonic crystal slab system naturally satisfies the considerations as outlined above. By using a pair of such high-quality-factor guided resonances and by applying a dynamic modulation with its modulation frequency and modulation wave-vector matching the frequency and momentum differences of these two resonances, we demonstrate theoretically and numerically that this device can break reciprocity in the optical range. In the lossless limit, one can achieve perfect optical circulation. Even with material loss that is realistic in the free-carrier-based modulation schemes in silicon, this device is still capable of attaining complete optical isolation with no back reflection.

As a concrete implementation, we consider in two dimensions a one-dimensional photonic crystal slab as shown in Figure 1a, which consists of a perfect electric conductor (PEC) substrate, an air superstrate, and a dielectric slab waveguide with periodic grooves along the $\hat{x}$-direction spaced at a periodicity of a = 550 nm. The dielectric slab has a thickness of 625 nm, and it has a relative permittivity of 11.56, which is similar to that of silicon in the optical range. The periodic grooves are 100 nm in width and 75 nm in height, and they have a relative permittivity of 12.25. Without loss of generality, we study the transverse magnetic (TM) polarization, where the nonzero field components are E_z, H_x, and H_y. We first focus our analysis by assuming no material loss is present, which enables this device to act as a perfect optical circulator. Then, we introduce material loss that may be associated with modulation and show that this device can still achieve complete optical isolation.

We start by analyzing the properties of this photonic crystal slab with no time-dependent permittivity modulation. Because of the periodicity along $\hat{x}$, according to Bloch's theorem, such a structure supports modes with the following form:[37−39]

$$E_z(x, y, t) = u_z(x, y)\mathrm{e}^{-\mathrm{i}Kx+\mathrm{i}\omega t} \quad (1)$$

where K is the Bloch wave vector in the $\hat{x}$-direction, which is real, $u_z(x, y)$ is the complex Bloch field profile that is periodic in $\hat{x}$, such that $u_z(x, y) = u_z(x + a, y)$, and ω is the complex frequency of the guided mode. For a photonic crystal slab made with lossless materials, the imaginary component of ω captures the rate at which the guided resonance mode radiates its power into free space.

With a standard frequency-domain eigenmode-solver technique,[37] we can numerically compute this photonic crystal slab's band diagram. We choose a spatial resolution of $\Delta x = \Delta y$ = 25 nm, and the band diagram is plotted on the left side of Figure 1b. This plot shows that around a frequency of 200 THz the

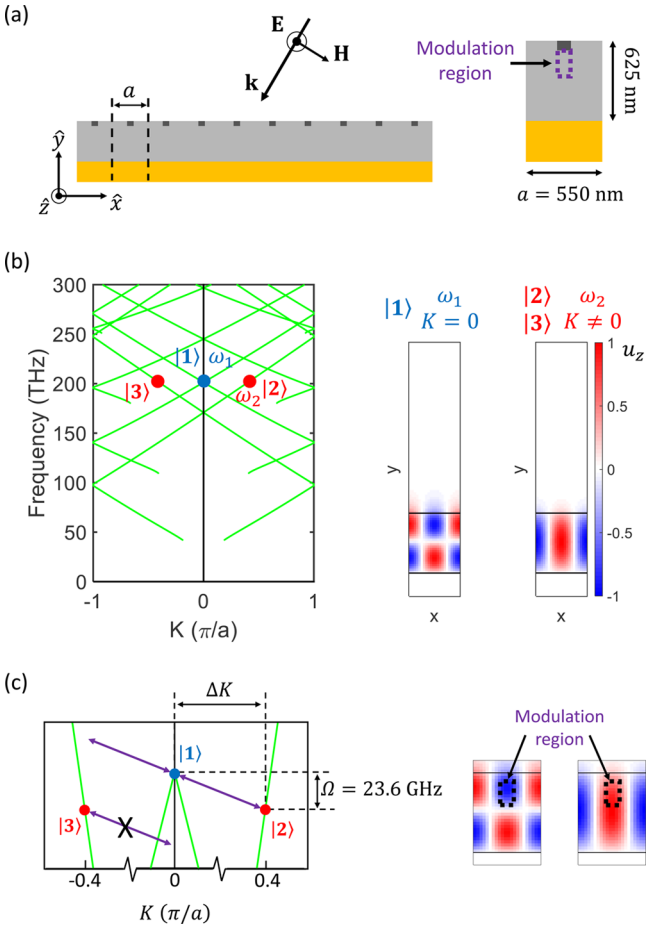

Figure 1. (a) Schematic of a photonic crystal slab and the geometry of one unit cell. (b) Left: Band structure of the photonic crystal slab, with the selected modes |1⟩, |2⟩, and |3⟩ labeled. Right: Bloch field profiles of the three modes. (c) Modulation can induce a photonic transition between modes |1⟩ and |2⟩ but not with |3⟩.

structure supports many different guided modes. For the purpose of subsequent discussions, we highlight three independent modes, which are labeled in Figure 1b. The mode labeled |1⟩ has a frequency $\omega_1 = 2\pi \times 201.1461$ THz and a wave-vector $K_1 = 0$, the mode labeled |2⟩ has a frequency $\omega_2 = 2\pi \times 201.1225$ THz and a wave-vector $K_2 = 0.4\pi/a$, and the mode labeled |3⟩ has the same frequency ω_2 as mode |2⟩ and a wave-vector $K_3 = -K_2 = -0.4\pi/a$. From the same eigenmode solver, we deduce that, due to radiative loss, mode |1⟩ has a quality factor of $Q_1 = 1.90 \times 10^5$ and resonance line width $2\gamma_1$ = 1.1 GHz, and modes |2⟩ and |3⟩ have quality factors of $Q_2 = Q_3 = 1.05 \times 10^6$ and resonance line width $2\gamma_2 = 2\gamma_3$ = 0.2 GHz. On the right side of Figure 1b, we show the Bloch field profiles $u_z(x, y)$ of these guided resonances. With respect to the center plane of the slab in the x−z plane, mode |1⟩ is approximately odd and modes |2⟩ and |3⟩ are approximately even. Furthermore, modes |2⟩ and |3⟩ have the same field profile due to mirror symmetry. Mode |1⟩ couples to normally incident and out-going plane waves, whereas mode |2⟩ (|3⟩) couples to obliquely incident and out-going plane waves with positive (negative) horizontal wave-vectors.

Following the concepts of ref 28, the reciprocity in this system can be broken by creating an indirect photonic transition between modes |1⟩ and |2⟩, which can be realized by applying a dynamic modulation to the permittivity in the

DOI: 10.1021/acsphotonics.7b00420
ACS Photonics 2017, 4, 1639−1645

regions, as indicated by the dashed lines in Figure 1a. These regions are chosen such that there is a significant overlap of the two modes integrated over the modulation region, as shown in Figure 1c. Mathematically, the permittivity of the modulated structure is described by[27,28]

$$\epsilon(x, y, t) = \epsilon_s(x, y) + \delta(x, y)\cos(\Omega t + \phi(x, y)) \quad (2)$$

where $\epsilon_s(x, y)$ is the time-independent permittivity profile of the device, $\delta(x, y)$ describes the spatial distribution of the modulation strength, Ω is the modulation frequency such that $\Omega = \omega_1 - \omega_2 = 2\pi \times 23.6$ GHz, and $\phi(x, y)$ is a spatially varying modulation phase profile that is chosen to satisfy the phase-matching condition: $\frac{\partial\phi}{\partial x} = K_2 - K_1 \equiv \Delta K$. It is well known that this type of permittivity modulation breaks Lorentz reciprocity.[27−34] As seen from Figure 1c, this modulation can drive a transition between modes $|1\rangle$ and $|2\rangle$, since the modulation satisfies the phase-matching condition for such a transition. On the other hand, this modulation cannot drive the transition between modes $|1\rangle$ and $|3\rangle$ due to phase mismatch.

Having discussed some of the properties of photonic transitions in our photonic crystal slab, we now show that such a photonic transition can be used to construct an optical circulator. Shown in Figure 2, we consider the response of our

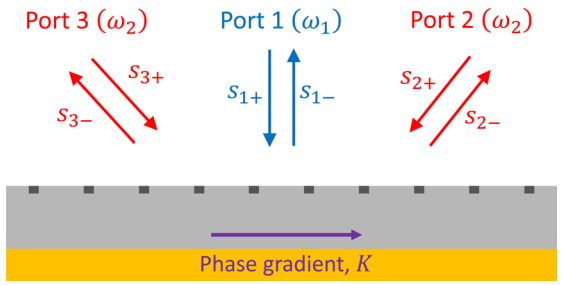

Figure 2. Setup of the three ports for optical circulation.

modulated structure to input/output waves in three ports. We define port 1 as a plane wave at frequency ω_1 that is propagating along the direction normal to the slab, port 2 as a plane wave at frequency ω_2 that is obliquely incident or out-going from the right, and port 3 as a plane wave at frequency ω_2 that is obliquely incident or out-going from the left. The labels $s_{m\pm}$, with $m = 1, 2, 3$, correspond to either an incident (+) or out-going (−) wave amplitude at each port. With this definition, under the condition that $\Omega \gg \gamma_1, \gamma_2$, mode $|1\rangle$ couples to $s_{1\pm}$, mode $|2\rangle$ couples to s_{2-} and s_{3+}, and mode $|3\rangle$ couples to s_{2+} and s_{3-}. When the slab is modulated as described above, the input amplitude s_{1+} can scatter into the output amplitude s_{2-} through a photonic transition from $|1\rangle$ to $|2\rangle$, whereas the input amplitude s_{2+} can scatter into the output amplitude s_{3-} but cannot scatter into the output amplitude s_{1-} due to the absence of photonic transition from $|3\rangle$ to $|1\rangle$. Furthermore, the input amplitude s_{3+} can scatter into s_{1-} through photonic transition from $|2\rangle$ to $|1\rangle$. Therefore, this device can function as a three-port optical circulator.

Mathematically, one can describe the modulated device using the temporal coupled mode theory (CMT).[40] With the rotating wave approximation,[27] the dynamics of the modes and their interactions with the input and out-going wave amplitudes in the ports can be written as

$$\begin{aligned}
\dot{a}_1 &= (i\omega_1 - \gamma_1^{rad} - \gamma_1^{loss})a_1 + i\kappa e^{-i\Omega t}a_2 + \sqrt{2\gamma_1^{rad}}s_{1+},\\
\dot{a}_2 &= (i\omega_2 - \gamma_2^{rad} - \gamma_2^{loss})a_2 + i\kappa e^{i\Omega t}a_1 + \sqrt{2\gamma_2^{rad}}s_{3+},\\
\dot{a}_3 &= (i\omega_2 - \gamma_3^{rad} - \gamma_3^{loss})a_3 + \sqrt{2\gamma_3^{rad}}s_{2+},\\
s_{1-} &= -s_{1+} + \sqrt{2\gamma_1^{rad}}a_1,\\
s_{2-} &= -s_{3+} + \sqrt{2\gamma_2^{rad}}a_2,\\
s_{3-} &= -s_{2+} + \sqrt{2\gamma_3^{rad}}a_3
\end{aligned} \quad (3)$$

where a_n is the amplitude of mode $|n\rangle$, γ_n^{rad} and γ_n^{loss} are the amplitude decay rate of mode $|n\rangle$ due to radiative coupling to input/output ports and dissipative loss, respectively, and κ denotes the coupling strength between the two modes induced by permittivity modulation. Due to inversion symmetry between modes $|2\rangle$ and $|3\rangle$, $\gamma_2^{rad,loss} = \gamma_3^{rad,loss}$. In this coupled mode theory formalism, the frequencies of the input waves in ports 1, 2, and 3 are assumed to be near the frequencies ω_1, ω_2, and ω_2, respectively. Moreover, we assume that the modulation frequency Ω is much larger than the decay rates γ's, so that the converted frequency components are well shifted from the incident frequency component.

We first analyze eq 3 in the lossless case where we set $\gamma_{1,2}^{loss} = 0$; that is, we assume that the decay from each mode radiatively couples to the respective ports. To extract the steady-state response, we consider an excitation of this system at an input frequency of ω so that a_n, $s_{n\pm} \sim e^{i\omega t}$. Upon making the substitutions

$$\begin{aligned}
&A_1 = a_1 e^{-i\Omega t/2},\ A_2 = a_2 e^{i\Omega t/2},\ A_3 = a_3 e^{-i\Omega t/2}\\
&S_{1\pm} = s_{1\pm} e^{-i\Omega t/2},\ S_{2\pm} = s_{2\pm} e^{i\Omega t/2},\ S_{3\pm} = s_{3\pm} e^{i\Omega t/2}
\end{aligned} \quad (4)$$

we can derive the scattering matrix of this system to be

$$\begin{pmatrix} S_{1-}\\ S_{2-}\\ S_{3-}\end{pmatrix} = \begin{pmatrix} \frac{2\gamma_1(i\Delta\omega + \gamma_2^{rad})}{D} - 1 & 0 & \frac{2i\kappa\sqrt{\gamma_1^{rad}\gamma_2^{rad}}}{D}\\ \frac{2i\kappa\sqrt{\gamma_1^{rad}\gamma_2^{rad}}}{D} & 0 & \frac{2\gamma_2(i\Delta\omega + \gamma_1^{rad})}{D} - 1\\ 0 & \frac{2\gamma_2^{rad}}{i\Delta\omega + \gamma_2^{rad}} - 1 & 0\end{pmatrix}\begin{pmatrix} S_{1+}\\ S_{2+}\\ S_{3+}\end{pmatrix} \quad (5)$$

where $\Delta\omega = \omega - \frac{\omega_1 + \omega_2}{2} \equiv \omega - \omega_0$ represents the frequency

DOI: 10.1021/acsphotonics.7b00420
ACS Photonics 2017, 4, 1639−1645

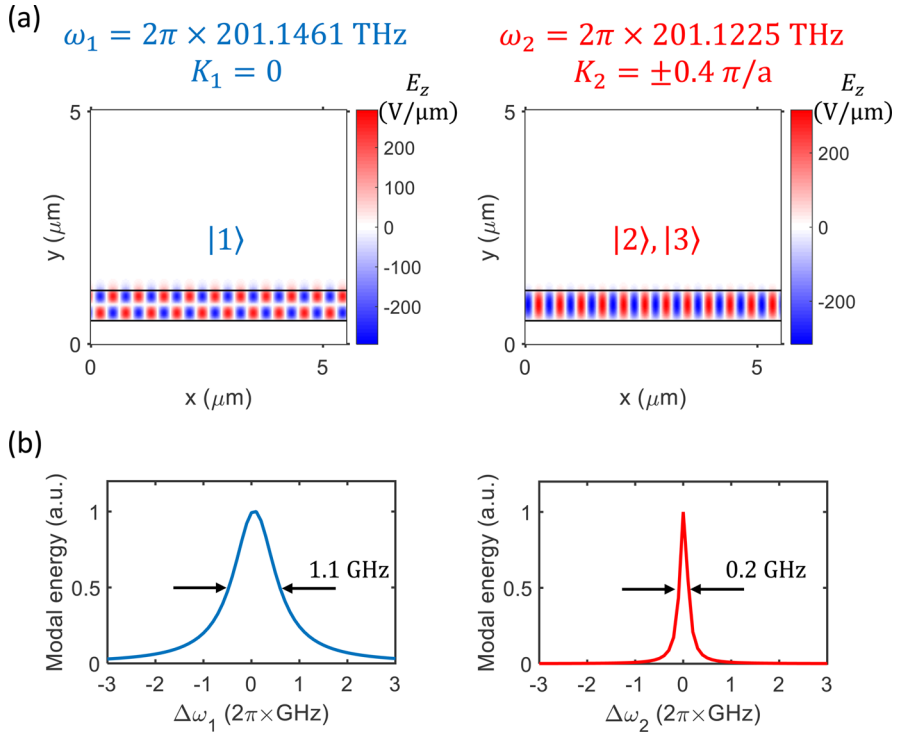

Figure 3. (a) Field profiles of the three modes as well as (b) their resonant line shapes. In this figure, $\omega_1 = 2\pi \times 201.1461$ THz and $\omega_2 = 2\pi \times 201.1225$ THz, whose separation is large enough (23.6 GHz) to resolve these modes in frequency, but small enough so that the photonic transition between these modes can be obtained from an electro-optic modulator.

detuning away from the photonic transition frequency, and $D = (i\Delta\omega + \gamma_1^{rad})(i\Delta\omega + \gamma_2^{rad}) + \kappa^2$. Under the conditions of on-resonance excitation

$$\Delta\omega = 0 \tag{6}$$

and critical coupling

$$\kappa^2 = \gamma_1^{rad}\gamma_2^{rad} \tag{7}$$

the scattering matrix becomes

$$\begin{pmatrix} S_{1-} \\ S_{2-} \\ S_{3-} \end{pmatrix} = \begin{pmatrix} 0 & 0 & i \\ i & 0 & 0 \\ 0 & 1 & 0 \end{pmatrix} \begin{pmatrix} S_{1+} \\ S_{2+} \\ S_{3+} \end{pmatrix} \tag{8}$$

Such an asymmetric scattering matrix clearly shows that Lorentz reciprocity is broken, and this device acts a perfect optical circulator.

Guided by the theoretical discussions above, we now perform full-wave simulations on the device in Figure 1a to demonstrate its ability to achieve perfect optical circulation. To simulate the modulated structure, we use the multifrequency finite-difference frequency-domain (FDFD) method as described in ref 41, which allows for the efficient first-principle simulations of such a modulated device with drastically different time scales. In order to describe the dynamic index modulation, the simulation domain consists of 10 unit cells of the device structure shown in Figure 1, and we apply periodic boundary conditions on the left and right boundaries. We implement the stretched-coordinate perfectly matched layers (SC-PMLs) at the top and bottom boundaries.[42] The spatial discretization is chosen to be $\Delta x = \Delta y = 25$ nm, which is the same as the calculation in Figure 1. In the absence of the dynamic index modulation, to find the guided resonances of this structure, we place a plane wave source at 2.85 μm above the structure. The source excites a plane wave with an electric field strength of 1 V/μm with either $K = 0$ (normal incidence) or $K = \pm 0.4\pi/a$ (incidence at $\pm$32.8 degrees from normal). In agreement with the band-structure calculation presented in Figure 1b, we find that mode $|1\rangle$ exists at $K_1 = 0$ with frequency $\omega_1 = 2\pi \times 201.1461$THz (corresponding to a wavelength $\lambda_1 = 1490.4$ nm) and line width $2\gamma_1 = 1.1$ GHz. Mode $|2\rangle$ exists at $K_2 = +0.4\pi/a$ at frequency $\omega_2 = 2\pi \times 201.1255$ THz (which corresponds to a wavelength $\lambda_2 = 1490.6$ nm) with line width $2\gamma_2 = 0.2$ GHz. In addition, mode $|3\rangle$ exists at $K_3 = -K_2 = -0.4\pi/a$ at frequency $\omega_3 = \omega_2$, as is required by symmetry. Importantly, ω_1 and ω_2 differ by 23.6 GHz $\gg \gamma_1, \gamma_2$, which makes it possible to spectrally resolve modes $|1\rangle$ with $|2\rangle$ and $|3\rangle$. Furthermore, time-dependent permittivity modulation at a frequency equal to the frequency separation between ω_1 and ω_2 is also achievable with silicon modulation technology.[36]

Next, we demonstrate numerically that with the appropriate permittivity modulation this device can function as a perfect optical circulator. Shown in Figure 1a, the modulation region is located directly underneath the bump region with a length of 250 nm. The size and the location of the modulation region are chosen such that there is a significant modal overlap between modes $|1\rangle$ and $|2\rangle$, $|3\rangle$, as integrated throughout the modulation region. In each unit cell, the modulation is applied uniformly according to eq 2 with a modulation strength of $\delta = 7.3 \times 10^{-4}$. This modulation strength is chosen such that the critical coupling condition of eq 7 is satisfied. The regions are modulated at a frequency $\Omega = \omega_1 - \omega_2 = 2\pi \times 23.6$ GHz. The modulation phases of the adjacent unit cells are chosen to differ by $\Delta\phi = 0.4\pi$. The choice of the modulation frequency and modulation phase distribution ensures that the modulation

DOI: 10.1021/acsphotonics.7b00420
ACS Photonics 2017, 4, 1639−1645

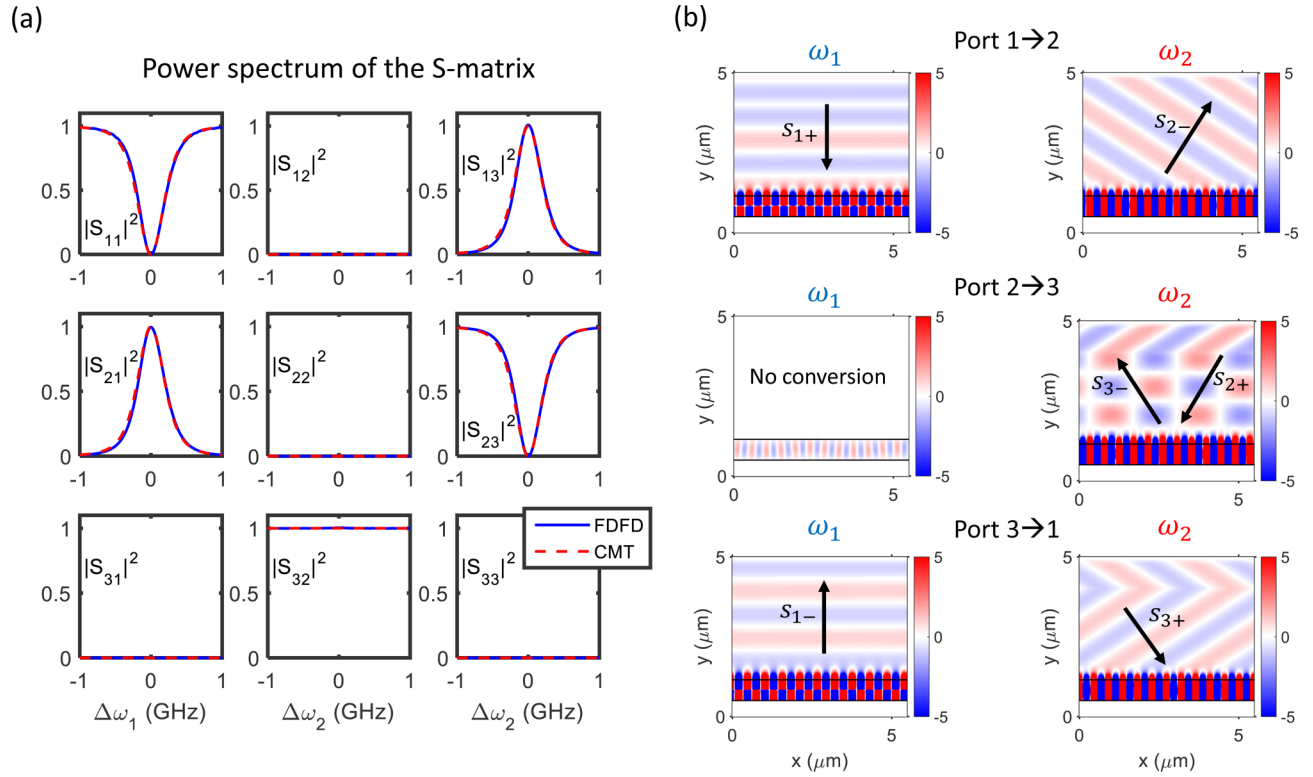

Figure 4. (a) Plot of the power spectrum of various *S*-matrix elements obtained from the multifrequency FDFD simulations and coupled mode theory calculations. The theory and the simulations show excellent agreement. On resonance with $\Delta\omega_{1,2} = 0$, we obtain the ideal scattering matrix for optical circulation. (b) Field plots of the optical circulator showing perfect conversion with no back reflection.

satisfies the phase-matching condition in order to induce the transition from $|1\rangle$ to $|2\rangle$.

With the multifrequency FDFD algorithm, we can obtain for this system the *S*-matrix, i.e., the matrix elements of the scattering matrix that characterizes the input−output relations. In three separate sets of simulations, we send in incoming waves from ports s_{1+}, s_{2+}, and s_{3+}, respectively, and obtain the power spectra of the *S*-matrix by varying the frequency of the incoming waves as shown in Figure 4a. The input frequency detuned away from the resonant frequencies of the guided resonance modes is represented by $\Delta\omega_{1,2} = \omega - \omega_{1,2}$. The numerically obtained spectra agree very well with the coupled mode theory calculations as described in eq 5 using the parameters described above that are obtained from the simulations of the static structure. Several of the spectra shown in Figure 4a exhibit a strong resonant behavior, which corresponds to the excitation of the guided resonance associated with each individual input port. Far away from the resonance, the *S*-matrix approaches the form $\begin{pmatrix} 1 & 0 & 0 \\ 0 & 0 & 1 \\ 0 & 1 & 0 \end{pmatrix}$, which is symmetric, as is typical for a reciprocal reflector. When $\Delta\omega_{1,2} = 0$, as a result of the resonant excitation of mode $|1\rangle$ and the perfect photonic transition between modes $|1\rangle$ and $|2\rangle$, the *S*-matrix takes the form $\begin{pmatrix} 0 & 0 & 1 \\ 1 & 0 & 0 \\ 0 & 1 & 0 \end{pmatrix}$, which is the *S*-matrix for a perfect optical circulator. From the same calculation, we find that the 3 dB bandwidth is 400 MHz, which is limited by the intrinsic quality factor of the guided resonance modes.

Moreover, in Figure 4b, we show the steady-state field profiles when we send in waves into each input port on resonance. The incoming wave from port 1 at ω_1 is completely scattered into the out-going wave at ω_2 into port 2 through photonic transition. The incoming wave at ω_2 from port 2 goes to port 3 through reflection with no frequency conversion, which indicates the absence of photonic transition. The incoming wave at ω_2 from port 3 is completely scattered into the out-going wave at ω_1 at port 1 via photonic transition. In addition, each of these scattering events incurs no back reflection. The simulations indeed demonstrate the behavior of a perfect optical circulator. We note that this meta-surface has a linear response with respect to the amplitudes of the incoming wave; it is therefore not subjected to the limitations as imposed by dynamic reciprocity in the class of nonlinear reciprocity-breaking devices.[22]

In all the calculations and simulations above, we assumed that the loss of the resonance comes entirely from radiation to the output ports. The material itself is lossless, and the modulation does not incur any absorptive loss. Such a low-loss modulation can be achieved using electro-optic effects in materials such as GaAs and $LiNbO_3$.[43] On the other hand, in a material like silicon, electro-optic modulation is typically carried out by manipulating free-carrier concentration or distribution.[36,44] The presence of free carriers inevitably introduces absorptive loss. In order to construct optical devices that are compatible with CMOS technology for integration onto silicon chips, it is important to characterize how such a free-carrier absorption loss affects the performance of the envisioned nonreciprocal device. Here, we will show that with loss that is inherently associated with the required modulation depth, our device still exhibits strong nonreciprocal response.

To describe the effect of loss, we first estimate the magnitude of material loss based on the modulation depth.[44] In our dynamic simulation as described below, we will use a

DOI: 10.1021/acsphotonics.7b00420
ACS Photonics 2017, 4, 1639−1645

modulation strength of $\delta = 8.3 \times 10^{-4}$, which can be achieved with a hole concentration of $N_p = 10^{17}$ cm^{-3}. Such a hole concentration in turn induces an imaginary permittivity of $\epsilon_I = 6.5 \times 10^{-5}$ in the modulation region.[44] We note that the modulation strength here is slightly increased as compared to the lossless case in order to achieve optimal performance for the optical isolation in the lossy case. We now repeat the full wave simulations of this device as we did for Figures 3 and 4 by adding the imaginary ϵ_I mentioned above inside the modulation region to account for material loss. In the simulation of the time-independent device, we find that the line widths of all the modes were broadened by $\gamma_{1,2}^{loss} = 2\pi \times 0.05$ GHz, which is smaller than the radiation loss rates γ_1^{rad} and γ_2^{rad}. We repeat the modulation simulation with loss using the multifrequency FDFD at a modulation strength of $\delta = 8.3 \times 10^{-4}$ (which does not significantly affect $\gamma_{1,2}^{loss}$) and plot the power spectrum of the S-matrix in Figure 5. At the same time, we plot the power spectrum of the coupled mode theory calculations from eq 3 by including $\gamma_{1,2}^{loss}$, which agrees very well with the FDFD results. We observe that even under loss the power spectrum of the S-matrix shows that, near the resonance of photonic transition, full isolation can still be attained between ports 1 and 2 or ports 1 and 3, although the insertion loss is increased due to dissipation. From the same figure, however, we see that the same device can no longer function as a perfect optical circulator because $|S_{23}|$ and $|S_{32}|$ are becoming more symmetric due to material loss.

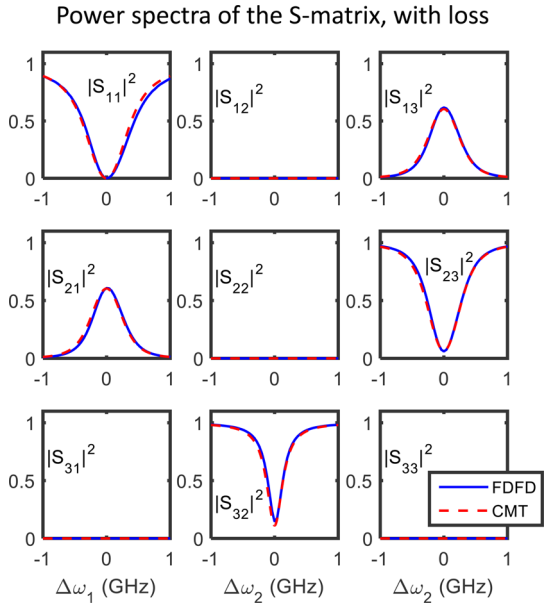

Figure 5. Plot of the power spectrum of the S-matrix in the presence of material loss due to modulation. Both the multifrequency FDFD simulations and CMT results are included, which show excellent agreement. Full isolation can be achieved between ports 1 and 2 or ports 1 and 3, but ports 2 and 3 are becoming more reciprocal.

In all the analyses above, as a proof of principle we performed two-dimensional numerical computations with a one-dimensional photonic crystal slab under TM polarization. However, the coupled mode theory formalism is general, and hence the concept should be applicable to the TE polarization as well as to three-dimensional structures with a two-dimensional photonic crystal slab. As long as the photonic crystal slab is designed to support multiple guided resonance bands near the operating frequency, one can always find two guided resonance modes that are separated by a few gigahertz in frequency. Therefore, it is always possible to design a modulation to induce photonic transition between such guided resonance modes. In the simulation, we used a perfect electric conductor mirror for numerical convenience. In practice, one can use a one-dimensional Bragg reflector that provides near-complete reflection with negligible loss. In implementing the required modulation, one can consider a modulator structure that consists of PIN junctions,[36] where the intrinsic (I) regions occupy most of the slab structure, and the P and N regions are made sufficiently small as to reduce the contributions to material loss from these more heavily doped regions. A modulation array consisting of multiple PIN junctions with all modulators operating at the same frequency, and with separate phase control of the modulators, has been demonstrated in ref 29. Such a technology can be used for our purposes here as well.

In summary, we introduce a realistic dynamic meta-surface that breaks Lorentz reciprocity and can achieve optical circulation and isolation. This work combines the features of guided resonances of a photonic crystal slab and a dynamic modulation, and it should prove to be a step forward in the construction of nonreciprocal meta-surfaces for optical wave manipulation.

AUTHOR INFORMATION

Corresponding Author

*E-mail: shanhui@stanford.edu.

Notes

The authors declare no competing financial interest.

ACKNOWLEDGMENTS

We gratefully acknowledge the fruitful discussions with Qian Lin and Momchil Minkov. This work is supported by Samsung Electronics. Y.S. also acknowledges the support from a Stanford Graduate Fellowship.

REFERENCES

(1) Yu, N.; Capasso, F. Flat Optics with Designer Metasurfaces. *Nat. Mater.* **2014**, *13* (2), 139−150.

(2) Yu, N.; Genevet, P.; Kats, M. A.; Aieta, F.; Tetienne, J.-P.; Capasso, F.; Gaburro, Z. Light Propagation with Phase Discontinuities: Generalized Laws of Reflection and Refraction. *Science* **2011**, *334* (6054), 333−337.

(3) Kildishev, A. V.; Boltasseva, A.; Shalaev, V. M. Planar Photonics with Metasurfaces. *Science* **2013**, *339* (6125), 1232009.

(4) Lin, D.; Fan, P.; Hasman, E.; Brongersma, M. L. Dielectric Gradient Metasurface Optical Elements. *Science* **2014**, *345* (6194), 298−302.

(5) Verslegers, L.; Catrysse, P. B.; Yu, Z.; White, J. S.; Barnard, E. S.; Brongersma, M. L.; Fan, S. Planar Lenses Based on Nanoscale Slit Arrays in a Metallic Film. *Nano Lett.* **2009**, *9* (1), 235−238.

(6) Huang, Y.-W.; Lee, H. W. H.; Sokhoyan, R.; Pala, R. A.; Thyagarajan, K.; Han, S.; Tsai, D. P.; Atwater, H. A. Gate-Tunable Conducting Oxide Metasurfaces. *Nano Lett.* **2016**, *16* (9), 5319−5325.

(7) Papakostas, A.; Potts, A.; Bagnall, D. M.; Prosvirnin, S. L.; Coles, H. J.; Zheludev, N. I. Optical Manifestations of Planar Chirality. *Phys. Rev. Lett.* **2003**, *90* (10), 107404.

(8) Yu, N.; Aieta, F.; Genevet, P.; Kats, M. A.; Gaburro, Z.; Capasso, F. A Broadband, Background-Free Quarter-Wave Plate Based on Plasmonic Metasurfaces. *Nano Lett.* **2012**, *12* (12), 6328−6333.

(9) Shitrit, N.; Bretner, I.; Gorodetski, Y.; Kleiner, V.; Hasman, E. Optical Spin Hall Effects in Plasmonic Chains. *Nano Lett.* **2011**, *11* (5), 2038−2042.

DOI: 10.1021/acsphotonics.7b00420
ACS Photonics 2017, 4, 1639−1645

(10) Genevet, P.; Yu, N.; Aieta, F.; Lin, J.; Kats, M. A.; Blanchard, R.; Scully, M. O.; Gaburro, Z.; Capasso, F. Ultra-Thin Plasmonic Optical Vortex Plate Based on Phase Discontinuities. *Appl. Phys. Lett.* **2012**, *100* (1), 013101.
(11) Chen, S.; Fan, F.; Wang, X.; Wu, P.; Zhang, H.; Chang, S. Terahertz Isolator Based on Nonreciprocal Magneto-Metasurface. *Opt. Express* **2015**, *23* (2), 1015−1024.
(12) Hadad, Y.; Davoyan, A. R.; Engheta, N.; Steinberg, B. Z. Extreme and Quantized Magneto-Optics with Graphene Meta-Atoms and Metasurfaces. *ACS Photonics* **2014**, *1* (10), 1068−1073.
(13) Shaltout, A.; Kildishev, A.; Shalaev, V. Time-Varying Metasurfaces and Lorentz Non-Reciprocity. *Opt. Mater. Express* **2015**, *5* (11), 2459−2467.
(14) Hadad, Y.; Sounas, D. L.; Alu, A. Space-Time Gradient Metasurfaces. *Phys. Rev. B: Condens. Matter Mater. Phys.* **2015**, *92* (10), 100304.
(15) Mahmoud, A. M.; Davoyan, A. R.; Engheta, N. All-Passive Nonreciprocal Metastructure. *Nat. Commun.* **2015**, *6*, 8359.
(16) Shi, Y.; Fan, S. Dynamic Non-Reciprocal Meta-Surfaces with Arbitrary Phase Reconfigurability Based on Photonic Transition in Meta-Atoms. *Appl. Phys. Lett.* **2016**, *108* (2), 021110.
(17) Taravati, S.; Khan, B. A.; Gupta, S.; Achouri, K.; Caloz, C.Nonreciprocal Nongyrotropic Magnetless Metasurface *ArXiv160807324 Phys.*, 2016
(18) Correas-Serrano, D.; Gomez-Diaz, J. S.; Sounas, D. L.; Hadad, Y.; Alvarez-Melcon, A.; Alù, A. Nonreciprocal Graphene Devices and Antennas Based on Spatiotemporal Modulation. *IEEE Antennas Wirel. Propag. Lett.* **2016**, *15*, 1529−1532.
(19) Hadad, Y.; Soric, J. C.; Alu, A. Breaking Temporal Symmetries for Emission and Absorption. *Proc. Natl. Acad. Sci. U. S. A.* **2016**, *113* (13), 3471−3475.
(20) Haus, H. A. *Waves and Fields in Optoelectronics*; Prentice Hall: Englewood Cliffs, NJ, 1983.
(21) Jalas, D.; Petrov, A.; Eich, M.; Freude, W.; Fan, S.; Yu, Z.; Baets, R.; Popović, M.; Melloni, A.; Joannopoulos, J. D.; Vanwolleghem, M.; Doerr, C. R.; Renner, H. What Is — and What Is Not — an Optical Isolator. *Nat. Photonics* **2013**, *7* (8), 579−582.
(22) Shi, Y.; Yu, Z.; Fan, S. Limitations of Nonlinear Optical Isolators due to Dynamic Reciprocity. *Nat. Photonics* **2015**, *9* (6), 388−392.
(23) Tien, M.-C.; Mizumoto, T.; Pintus, P.; Kromer, H.; Bowers, J. E. Silicon Ring Isolators with Bonded Nonreciprocal Magneto-Optic Garnets. *Opt. Express* **2011**, *19* (12), 11740−11745.
(24) Shoji, Y.; Mizumoto, T. Magneto-Optical Non-Reciprocal Devices in Silicon Photonics. *Sci. Technol. Adv. Mater.* **2014**, *15* (1), 014602.
(25) Estep, N. A.; Sounas, D. L.; Soric, J.; Alù, A. Magnetic-Free Non-Reciprocity and Isolation Based on Parametrically Modulated Coupled-Resonator Loops. *Nat. Phys.* **2014**, *10* (12), 923−927.
(26) Dong, P.; Preble, S. F.; Robinson, J. T.; Manipatruni, S.; Lipson, M. Inducing Photonic Transitions between Discrete Modes in a Silicon Optical Microcavity. *Phys. Rev. Lett.* **2008**, *100* (3), 033904.
(27) Fang, K.; Yu, Z.; Fan, S. Photonic Aharonov-Bohm Effect Based on Dynamic Modulation. *Phys. Rev. Lett.* **2012**, *108* (15), 153901.
(28) Yu, Z.; Fan, S. Complete Optical Isolation Created by Indirect Interband Photonic Transitions. *Nat. Photonics* **2009**, *3* (2), 91−94.
(29) Lira, H.; Yu, Z.; Fan, S.; Lipson, M. Electrically Driven Nonreciprocity Induced by Interband Photonic Transition on a Silicon Chip. *Phys. Rev. Lett.* **2012**, *109* (3), 033901.
(30) Doerr, C. R.; Chen, L.; Vermeulen, D. Silicon Photonics Broadband Modulation-Based Isolator. *Opt. Express* **2014**, *22* (4), 4493−4498.
(31) Li, E.; Eggleton, B. J.; Fang, K.; Fan, S. Photonic Aharonov−Bohm Effect in Photon−phonon Interactions. *Nat. Commun.* **2014**, *5*, 3225.
(32) Tzuang, L. D.; Fang, K.; Nussenzveig, P.; Fan, S.; Lipson, M. Non-Reciprocal Phase Shift Induced by an Effective Magnetic Flux for Light. *Nat. Photonics* **2014**, *8* (9), 701−705.
(33) Taravati, S.; Caloz, C. Mixer-Duplexer-Antenna Leaky-Wave System Based on Periodic Space-Time Modulation. *IEEE Trans. Antennas Propag.* **2017**, *65* (2), 442−452.
(34) Winn, J. N.; Fan, S.; Joannopoulos, J. D.; Ippen, E. P. Interband Transitions in Photonic Crystals. *Phys. Rev. B: Condens. Matter Mater. Phys.* **1999**, *59* (3), 1551−1554.
(35) Wang, K.; Shi, Y.; Solntsev, A. S.; Fan, S.; Sukhorukov, A. A.; Neshev, D. N. Non-Reciprocal Geometric Phase in Nonlinear Frequency Conversion. *Opt. Lett.* **2017**, *42*, 1990−1993.
(36) Reed, G. T.; Mashanovich, G. Z.; Gardes, F. Y.; Nedeljkovic, M.; Hu, Y.; Thomson, D. J.; Li, K.; Wilson, P. R.; Chen, S.-W.; Hsu, S. S. Recent Breakthroughs in Carrier Depletion Based Silicon Optical Modulators. *Nanophotonics* **2013**, *3* (4−5), 229−245.
(37) Joannopoulos, J. D.; Johnson, S. G.; Winn, J. N.; Meade, R. D. *Photonic Crystals: Molding the Flow of Light* (2nd ed.); Princeton University Press, 2011.
(38) Johnson, S. G.; Fan, S.; Villeneuve, P. R.; Joannopoulos, J. D.; Kolodziejski, L. A. Guided Modes in Photonic Crystal Slabs. *Phys. Rev. B: Condens. Matter Mater. Phys.* **1999**, *60* (8), 5751−5758.
(39) Fan, S.; Joannopoulos, J. D. Analysis of Guided Resonances in Photonic Crystal Slabs. *Phys. Rev. B: Condens. Matter Mater. Phys.* **2002**, *65* (23), 235112.
(40) Suh, W.; Wang, Z.; Fan, S. Temporal Coupled-Mode Theory and the Presence of Non-Orthogonal Modes in Lossless Multimode Cavities. *IEEE J. Quantum Electron.* **2004**, *40* (10), 1511−1518.
(41) Shi, Y.; Shin, W.; Fan, S. Multi-Frequency Finite-Difference Frequency-Domain Algorithm for Active Nanophotonic Device Simulations. *Optica* **2016**, *3* (11), 1256−1259.
(42) Berenger, J.-P. A Perfectly Matched Layer for the Absorption of Electromagnetic Waves. *J. Comput. Phys.* **1994**, *114* (2), 185−200.
(43) Yariv, A.; Yeh, P. *Optical Waves in Crystals: Propagation and Control of Laser Radiation*; Wiley, 1984.
(44) Soref, R.; Bennett, B. Electrooptical Effects in Silicon. *IEEE J. Quantum Electron.* **1987**, *23* (1), 123−129.

DOI: 10.1021/acsphotonics.7b00420
ACS Photonics 2017, 4, 1639−1645